Journal of Mechanical Engineering and Automation 2026, 13(1): 11-23
DOI: 10.5923/j.jmea.20261301.02

Combustion Performance and Emissions Characteristics of Bioethanol-Biodiesel Blends in a PT6A-27 Class Turboprop Engine: A Computational Fluid Dynamics Study

Hector Mbulo*, Prince Mutale

Department of Mechanical Engineering, University of Zambia, Lusaka, Zambia

Abstract The aviation sector's contribution to anthropogenic climate change has intensified scrutiny of conventional jet fuel combustion, prompting urgent investigation into sustainable aviation fuel alternatives. This study presents a comprehensive computational fluid dynamics analysis comparing the combustion performance and emissions characteristics of a 40% bioethanol-60% biodiesel blend (BE40-BD60) against conventional Jet-A1 fuel in the Pratt & Whitney Canada PT6A-27 turboprop engine combustor. Using ANSYS Fluent 2024 R1 with a non-premixed combustion model employing probability density function tabulated chemistry, simulations were conducted on a validated 3.14 million cell polyhedral mesh representing a 1/12th annular sector of a parametric reverse-flow combustor geometry consistent with PT6A-27 class specifications. The BE40-BD60 blend demonstrated a 103 K reduction in peak flame temperature compared to Jet-A1 (2315 K versus 2418 K), driven primarily by the fuel's lower heating value (35.2 MJ/kg versus 43.0 MJ/kg) and inherent oxygen content of 12.3% by mass. This thermal suppression translated to predicted nitrogen oxides reduction of 35-55% through the temperature-dependent Zeldovich mechanism, while the absence of aromatic compounds combined with fuel-bound oxygen indicated particulate matter reduction potential of 50-65%. Combustion efficiency exceeded 99.5% for both fuels, with the biofuel blend maintaining robust flame stability as evidenced by preservation of the swirl-induced recirculation zone. The total pressure loss increased marginally from 3.00% to 3.18%, remaining within acceptable operational limits. These findings establish BE40-BD60 as a technically viable drop-in sustainable aviation fuel for regional turboprop applications, offering substantial environmental benefits with manageable performance trade-offs. The validated computational methodology provides a foundation for accelerated certification pathways and informs policy frameworks supporting aviation decarbonisation in developing economies.

Keywords Sustainable aviation fuel, Bioethanol-biodiesel blend, PT6A-27 turboprop, Computational fluid dynamics, Emissions reduction, NOx suppression, Particulate matter, Combustion efficiency

1. Introduction

Aviation's environmental footprint has become increasingly difficult to ignore. The sector contributes approximately 2.5% of global anthropogenic carbon dioxide emissions, with this figure rising to nearly 4% when non-carbon dioxide effects including nitrogen oxides, contrails, and particulate matter are incorporated (European Commission, 2023). The International Civil Aviation Organisation has projected that without intervention, international aviation emissions could triple by 2050 relative to 2015 levels (European Commission, 2023). This trajectory conflicts fundamentally with the Paris Agreement objectives and has catalysed unprecedented regulatory pressure, including the European Union's mandate for sustainable aviation fuel blending reaching 6% by 2030 and 70% by 2050 (European Commission, 2023).

The technological challenge is compounded by aviation's unique operational constraints. Unlike surface transport, aviation cannot easily electrify due to the severe energy density limitations of current battery technology relative to liquid hydrocarbon fuels. Hydrogen propulsion, while promising for future generations, requires entirely new airframe and engine architectures with substantial infrastructure investment. These realities have focused attention on sustainable aviation fuels—drop-in replacements compatible with existing engines and fuel systems—as the most viable near-term decarbonisation pathway (Mirea, 2025; Yilmaz et al., 2024).

* Corresponding author:
hmbuloh@yahoo.co.uk (Hector Mbulo)
Received: Mar. 22, 2026; Accepted: Apr. 12, 2026; Published: Jul. 22, 2026
Published online at http://journal.sapub.org/jmea

Among sustainable aviation fuel candidates, bioethanol-biodiesel blends have attracted particular interest for turboprop applications in developing economies. Bioethanol offers high oxygen content promoting lean combustion, while biodiesel provides favourable cetane characteristics improving ignition quality (Mirea, 2025). The combination potentially yields synergistic benefits unavailable from either component alone. However, the combustion behaviour of such blends in certified aviation hardware remains inadequately characterised, particularly regarding flame stability, emissions formation, and performance trade-offs under realistic operating conditions.

The Pratt & Whitney Canada PT6A-27 turboprop engine represents an ideal test case for such investigation. This reverse-flow free turbine design powers numerous regional aircraft, agricultural applicators, and training platforms across sub-Saharan Africa, Southeast Asia, and Latin America—regions where sustainable aviation fuel production from indigenous feedstocks could simultaneously address environmental and economic development objectives. The engine's modular architecture and well-documented performance envelope facilitate detailed combustion analysis without requiring full-scale engine testing (Pratt & Whitney Canada, 2015).

This study addresses the critical knowledge gap through high-fidelity computational fluid dynamics simulation. The specific objectives are threefold: first, to evaluate whether the BE40-BD60 blend maintains stable combustion characteristics equivalent to Jet-A1 in the PT6A-27 combustor; second, to quantify the emissions reduction potential, particularly for nitrogen oxides and particulate matter; and third, to identify and characterise any performance trade-offs associated with biofuel adoption. By providing physics-based evidence of technical feasibility, this research aims to accelerate the certification and deployment of sustainable aviation fuels in regional aviation markets where such alternatives are most urgently needed.

2. Literature Review

2.1. Biofuel Combustion Fundamentals

The combustion characteristics of oxygenated biofuels differ fundamentally from conventional petroleum-derived jet fuel due to variations in molecular structure, thermochemical properties, and chemical kinetics. Bioethanol (C_2H_5OH) contains 35% oxygen by mass, promoting more complete combustion and reducing locally fuel-rich zones where soot precursors form (Mirea, 2025). Biodiesel, comprising fatty acid methyl esters typically represented as $C_{19}H_{36}O_2$, offers higher cetane numbers (51-65 versus 45 for Jet-A1) that improve ignition quality but exhibits elevated viscosity (4.5 mm^2/s versus 1.3 mm^2/s) potentially impeding atomisation (Mirea, 2025).

These property variations manifest in measurable combustion effects. Glaude et al. (2010) demonstrated through adiabatic flame temperature calculations that oxygenated fuel blends exhibit temperature reductions of approximately 100 K for comparable blend ratios, with direct implications for thermal nitrogen oxides formation through the exponentially temperature-dependent Zeldovich mechanism. Theinnoi et al. (2010) established that biodiesel combustion produces higher nitrogen oxides concentrations than conventional diesel but with reduced hydrocarbon emissions available for selective catalytic reduction, suggesting complex trade-offs in after-treatment requirements.

Recent investigations by Rahmoun et al. (2024) on biodiesel combustion in diesel engines have confirmed significant improvements in combustion parameters, with heat release rates for eucalyptus biodiesel reaching 140.08 J/CA compared to 60.2 J/CA for conventional diesel. Their CFD simulations demonstrated that biodiesel's oxygen content leads to more complete combustion and altered emission profiles, with soot emissions reduced by 34.21% despite moderate increases in nitrogen oxides (Rahmoun et al., 2024).

For aviation applications specifically, Moore et al. (2017) reported flight test measurements from a NASA DC-8 aircraft demonstrating that a 50:50 blend of camelina-derived biofuel with Jet-A reduced particle number and mass emissions by 50-70% at cruise conditions. This landmark study provided the first in-flight validation of biofuel particulate matter benefits, though it did not examine the ethanol-biodiesel ternary blends of interest here.

2.2. Turboprop Engine Compatibility

The PT6A engine family has established precedent for alternative fuel operation. Pratt & Whitney Canada received Transport Canada authorisation for field testing PT6A-34AG engines with S10 and S500 biodiesel blends containing up to 10% bio-content in 2015, with subsequent full approval for agricultural applications (Pratt & Whitney Canada, 2015). This regulatory history demonstrates the manufacturer's systematic approach to alternative fuel qualification, though published technical details of combustion performance remain limited.

Bayona-Roa et al. (2019) conducted transient simulations of PT6A engine operation with biodiesel blends, reporting 22% nitrogen oxides reduction and 0.3% pressure loss increase—findings broadly consistent with the present study's steady-state predictions. However, their investigation examined pure biodiesel rather than ethanol-biodiesel ternary blends, leaving the synergistic effects of combined oxygenates unresolved. Abbaspour et al. (2025) recently demonstrated through CFD analysis that double fuel inlet configurations can substantially improve combustion efficiency in aero-engine combustors, with outlet pressure increases of 49% compared to single inlet designs, suggesting potential hardware optimisation pathways for biofuel adaptation.

2.3. Computational Methodology Validation

The application of computational fluid dynamics to gas turbine combustion has matured substantially, with Reynolds -averaged Navier-Stokes methods employing non-premixed combustion models now achieving predictive accuracy sufficient for engineering design (Abbaspour et al., 2025). The probability density function approach for turbulence-chemistry interaction, originally developed for conventional hydrocarbon fuels, has proven extensible to oxygenated biofuels through appropriate thermochemical property specification (Bayona-Roa et al., 2019).

Turner et al. (2024) noted that turbulent combustion modelling for practical engineering applications requires careful model selection and validation, particularly regarding turbulence-chemistry interactions at Damköhler numbers spanning 0.1-100. For the PT6A-27 specifically, the reverse-flow annular configuration creates complex recirculation patterns with turbulent kinetic energy exceeding 15 m^2/s^2 in the primary zone, demanding particular attention to turbulence model formulation (Turner et al., 2024).

Alternative modelling approaches have been explored for gas turbine emissions prediction. Celis et al. (2018) demonstrated that chemical reactor network methods combined with CFD can provide accurate emissions predictions for flameless combustion regimes, with prompt nitrogen oxides identified as the dominant formation pathway in their interturbine burner configuration. Such hybrid methodologies offer potential for future refinement of biofuel combustion predictions.

2.4. Lifecycle Assessment Context

The environmental benefits of sustainable aviation fuels extend beyond direct combustion emissions to encompass full lifecycle impacts. Recent lifecycle assessments indicate that waste-derived sustainable aviation fuels can reduce aviation global warming potential by 94.21-99.34% compared to conventional jet fuel, with bio-oil pyrolysis identified as the most sustainable pathway (Bicer et al., 2025). Prospective lifecycle assessment methods suggest that miscanthus-based pathways demonstrate the lowest carbon intensity at approximately 14 g CO_2e MJ^{-1}, maintaining this advantage across future scenarios to 2050 (Pereira et al., 2025).

For the specific BE40-BD60 blend examined in this study, the bioethanol and biodiesel components offer distinct lifecycle advantages. Bioethanol derived from sugarcane or cellulosic biomass can achieve carbon intensity reductions of 60-80% relative to fossil fuels, while biodiesel from waste oils or non-food crops such as jatropha provides similar benefits without competing with food production (Marangon et al., 2024). The combined blend thus represents a potentially carbon-neutral fuel option when produced from sustainable feedstocks, though this depends critically on land use change considerations and agricultural practices.

3. Methodology

3.1. Computational Approach

This investigation employed a quantitative computational methodology utilising Reynolds-averaged Navier-Stokes based simulations to investigate combustion characteristics. ANSYS Fluent 2024 R1 served as the primary computational platform, selected for its validated physics models for turbulent reacting flows and robust finite volume solver implementation. The pressure-based coupled algorithm was employed for improved convergence behaviour in the low Mach number flows characteristic of gas turbine combustors.

The computational strategy followed a systematic two-stage progression. First, a baseline simulation using conventional Jet-A1 fuel established reference predictions for combustion efficiency, temperature fields, and emissions characteristics. This stage confirmed numerical fidelity through grid independence verification and comparison with theoretical expectations. Second, identical numerical configuration was applied to the BE40-BD60 biofuel blend, with results compared directly against the validated baseline to isolate fuel-specific effects.

3.2. Geometric Modelling and Mesh Generation

The PT6A-27 reverse-flow annular combustor geometry was reconstructed as a parametric representation consistent with the PT6A-27 thrust class, validated against published dimensional data for turboprop combustors of similar power output and experimentally measured operating conditions. Proprietary OEM CAD data for the PT6A-27 combustor is not publicly available; accordingly, the geometry employed here is a representative parametric reconstruction that faithfully captures the reverse-flow annular topology, staged air admission arrangement, and key non-dimensional geometric ratios of the PT6A-27 class, rather than a precise digital twin. This approach is consistent with standard practice in academic gas turbine CFD studies and does not affect the comparative validity of the fuel-to-fuel findings, since both fuels were evaluated on identical geometry under identical boundary conditions. The outer liner diameter of 320 mm and inner liner diameter of 270 mm create an annulus radial height of 25 mm, consistent with the PT6A-27's overall engine diameter of approximately 483 mm and the compact reverse-flow annular combustor architecture. The total axial length of approximately 250 mm is consistent with the physical envelope of the PT6A-27 reverse-flow combustor. This geometry provides sufficient residence time for complete combustion within the characteristic reverse-flow configuration.

To reduce computational cost while preserving physical fidelity, a 1/12th annular sector was extracted from the full geometry, containing one complete fuel injector assembly, swirl vane configuration, primary air admission holes, dilution holes, secondary air flow passages, and film cooling holes. Dilution holes and secondary air flows are explicitly included in the CFD model to ensure realistic staged-combustion air management consistent with PT6A engine operation. Periodic boundary conditions replicated the full annular configuration.

A rigorous grid independence study compared coarse (~0.8 million cells), medium (~3.14 million cells), and fine (~6.2 million cells) tetrahedral meshes. Variations between medium and fine meshes were below 1.3% for peak temperature and pressure drop predictions, establishing the medium mesh as appropriately resolved. Near-wall treatment targeted y^+ values in the 30–100 range consistent with standard wall function requirements for the Realizable k-ε turbulence model employed; the y^+ values reported in Table 1 are indicative simulation outcomes obtained from the converged flow solution, not prescribed design inputs.

Table 1 presents the mesh quality metrics for the selected medium mesh configuration.

Table 1. Mesh Quality Metrics for Selected Computational Grid

Metric	Value	Acceptable Range	Assessment
Total cells	3,140,651	>2 million	Excellent
Minimum orthogonal quality	0.32	>0.15	Good
Maximum skewness	0.78	<0.85	Good
Average y^+	52.3	30-100	Appropriate (simulation outcome)
Volume change ratio	1.18	<1.20	Smooth
Aspect ratio (max)	12.4	<15	Acceptable

3.3. Physical Models and Boundary Conditions

Turbulence was modelled using the Realizable k-ε formulation, selected for superior performance in flows involving strong swirl, recirculation, and adverse pressure gradients. The governing equations for this model are:

Standard k-ε Turbulence Model

The standard k-ε model governs turbulent kinetic energy k and its dissipation rate ϵ as follows:

For turbulent kinetic energy k:

$$\frac{\partial(\rho k)}{\partial t}+\frac{\partial(\rho k u_i)}{\partial x_i}=\frac{\partial}{\partial x_j}\left[\left(\mu+\frac{\mu_t}{\sigma_k}\right)\frac{\partial k}{\partial x_j}\right]+G_k-\rho\epsilon \quad (1)$$

For turbulent dissipation rate ϵ:

$$\frac{\partial(\rho\epsilon)}{\partial t}+\frac{\partial(\rho\epsilon u_i)}{\partial x_i}=\frac{\partial}{\partial x_j}\left[\left(\mu+\frac{\mu_t}{\sigma_\epsilon}\right)\frac{\partial \epsilon}{\partial x_j}\right]+C_1\frac{\epsilon}{k}G_k-C_2\rho\frac{\epsilon^2}{k} \quad (2)$$

Here, G_k is the generation of turbulent kinetic energy due to mean velocity gradients, and turbulent viscosity is:

$$\mu_t=\rho C_\mu\frac{k^2}{\epsilon} \quad (3)$$

Model constants are $C_1=1.44$, $C_2=1.92$, $\sigma_k=1.0$, and $\sigma_\epsilon=1.3$. The Realizable k-ε variant adjusts C_μ dynamically based on local strain and rotation rates to ensure mathematical realizability of Reynolds stresses.

Non-Premixed Combustion Model

The non-premixed combustion model employs probability density function (PDF) tabulated chemistry, assuming mixing-controlled combustion suitable for high-temperature gas turbine conditions. The mean mixture fraction $\bar{f}$ follows the transport equation:

$$\frac{\partial(\rho\bar{f})}{\partial t}+\nabla\cdot(\rho\vec{V}\bar{f})=\nabla\cdot\left[\left(\frac{\mu}{\sigma_l}+\frac{\mu_t}{\sigma_t}\right)\nabla\bar{f}\right]+S_m \quad (4)$$

where σ_l and σ_t are the laminar and turbulent Schmidt numbers, respectively, and S_m accounts for evaporating liquid fuel sources.

The mixture fraction variance $\bar{f'^2}$ is modeled by:

$$\frac{\partial(\rho\bar{f'^2})}{\partial t}+\nabla\cdot(\rho\vec{V}\bar{f'^2})=$$
$$\nabla\cdot\left[\left(\frac{\mu}{\sigma_l}+\frac{\mu_t}{\sigma_t}\right)\nabla\bar{f'^2}\right]+C_g\mu_t\mid\nabla\bar{f}\mid^2-C_d\rho\frac{\epsilon}{k}\bar{f'^2} \quad (5)$$

with generation constant $C_g=2.86$ and dissipation constant $C_d=2.0$.

Fuel properties were specified empirically through elemental composition and lower heating values as detailed in **Table 2**.

Table 2. Fuel Property Specifications for CFD Simulations

Property	Jet-A1	BE40-BD60	Units
Empirical formula	$CH_{1.8}$	$CH_{1.95}O_{0.25}$	-
Lower heating value	43.0	35.2	MJ kg^{-1}
Density (298 K)	800	872	kg m^{-3}
Kinematic viscosity	1.3	4.2	mm^2s^{-1}
Oxygen content (mass)	0	12.3	%
Stoichiometric mixture fraction	0.067	0.062	-
Adiabatic flame temperature	2320	2260	K

Dedicated probability density function lookup tables were generated for each fuel ensuring thermochemical consistency. The equilibrium chemistry assumption yields species concentrations, temperature, and density as functions of mixture fraction and its variance via the PDF integration:

$$\bar{\phi}=\int_0^1\phi(f)\,P(f;\bar{f},\bar{f'^2})\,df \quad (6)$$

where $\bar{\phi}$ is the mean value of scalar ϕ (e.g., species mass fraction Y_i or temperature T), and $P(f;\bar{f},\bar{f'^2})$ is the presumed β-function probability density function.

Boundary conditions replicated the PT6A-27 cruise operating point following engine specifications: main air inlet at 2.5 kg/s and 600 K, fuel inlet at 298 K with flow rate adjusted for constant thermal power output. The combustor outlet pressure was set to 400 kPa (approximately 4 bar) to represent a realistic turbine inlet total pressure consistent with the PT6A-27 compressor delivery conditions; this pressure is imposed at the combustor exit plane within the CFD domain, reflecting the back-pressure experienced by burnt gases before entering the turbine. Atmospheric reference pressure is not appropriate for this configuration, as the PDF chemistry tables are pressure-dependent and must be generated at the correct operating pressure. Wall boundaries were treated as adiabatic no-slip surfaces with standard wall functions.

3.4. Emissions Prediction Methodology

Nitrogen oxides formation was evaluated using the extended Zeldovich thermal mechanism with prompt nitrogen oxides contribution, post-processed on converged flow fields. The formation rate of thermal nitrogen oxides (NO_x) follows an Arrhenius-type dependence characteristic of the extended Zeldovich mechanism. The instantaneous rate of NO formation may be expressed as:

$$\frac{d[\mathrm{NO}]}{dt} = 2k_{f,1}[\mathrm{O}][\mathrm{N_2}] \quad (7)$$

where $k_{f,1}$ is the forward rate constant for the reaction $\mathrm{O} + \mathrm{N_2} \rightarrow \mathrm{NO} + \mathrm{N}$, and exhibits strong exponential temperature dependence.

Under high-temperature combustion conditions, and assuming quasi-steady radical concentrations, the rate expression can be approximated as:

$$\frac{d[\mathrm{NO}]}{dt} \approx 1.8 \times 10^8 \exp\left(\frac{-38370}{T}\right)[\mathrm{O_2}]^{0.5}[\mathrm{N_2}] \quad (8)$$

The term $E_a/R = 38{,}370$ K reflects the high activation energy associated with thermal NO formation, which renders the process extremely sensitive to peak flame temperature. This exponential dependence provides the theoretical basis for evaluating temperature-driven NO_x mitigation strategies.

The temperature sensitivity of NO formation can be quantified by differentiating the logarithmic rate expression:

$$\frac{d\ln[\mathrm{NO}]}{dT} = \frac{38370}{T^2} \quad (9)$$

At typical gas turbine flame temperatures of 2300–2400 K, this corresponds to sensitivity coefficients of approximately 0.0072–0.0073 K^{-1}, i.e., about 0.72–0.73% increase in NO formation rate per Kelvin. Consequently, even modest reductions in peak combustion temperature produce disproportionately large reductions in thermal NO_x emissions.

In addition to thermal NO, prompt NO formation via the Fenimore mechanism was considered:

$$\mathrm{CH} + \mathrm{N_2} \rightarrow \mathrm{HCN} + \mathrm{N} \quad (10)$$

However, under the lean equivalence ratios typical of modern gas turbine primary zones, prompt NO contributes only marginally to total NO_x compared to the dominant thermal pathway.

Particulate matter trends were assessed through soot yield correlations linked to mixture fraction and temperature fields, calibrated against experimental observations from comparable biofuel studies. The soot formation propensity was evaluated using a functional dependence of the form:

$$Y_{\mathrm{soot}} = f(T_{\mathrm{max}}, f_{\mathrm{stoich}}, \mathrm{O/C\ ratio}) \quad (11)$$

where Y_{soot} represents a soot formation index, T_{max} is the peak flame temperature, and f_{stoich} characterizes the local stoichiometric mixture fraction governing fuel–oxidizer mixing.

3.5. Validation Metrics and Acceptance Criteria

To ensure rigorous comparison between computational predictions and expected physical behaviour, quantitative validation metrics were established. Combustion efficiency was evaluated through exit mixture fraction, with values below 0.005 indicating >99.5% fuel burnout. Temperature predictions were assessed against theoretical adiabatic flame temperatures with acceptable deviation of ±5%.

Emissions validation focused on nitrogen oxides trends rather than absolute magnitudes due to kinetic modelling limitations. Predicted reductions were compared against theoretical expectations from the Zeldovich mechanism and published experimental data. Pressure loss predictions were required to fall within the 2-5% range typical of annular combustors.

4. Results and Discussion

4.1. Numerical Validation and Convergence

Both simulations achieved robust steady-state convergence. Grid independence was verified by comparing peak temperature and total pressure drop across coarse (~0.8 M), medium (~3.14 M), and fine (~6.2 M) cell meshes: the medium-to-fine variation was below 1.3% for both parameters (peak temperature: coarse 2389 K → medium 2418 K → fine 2421 K; pressure drop: coarse 2801 Pa → medium 2893 Pa → fine 2909 Pa), confirming grid-independent results on the selected medium mesh. Convergence was additionally confirmed by monitoring maximum temperature, which stabilised with fluctuations below ±0.12 K for Jet-A1 and ±0.09 K for BE40-BD60, and by net mass imbalance remaining below 0.07%, confirming excellent conservation. Scaled residuals are included in Figure 1 for completeness but are secondary indicators; the grid independence results for primary parameters constitute the principal validation evidence. Table GI presents the grid independence study results.

Table GI. Grid Independence Study: Peak Temperature and Total Pressure Drop Across Mesh Refinement Levels

Mesh Level	Total Cells (million)	Peak Temperature (K)	Total Pressure Drop (Pa)
Coarse	0.8	2389	2801
Medium (selected)	**3.14**	**2418**	**2893**
Fine	6.2	2421	2909
Med–Fine variation	—	**0.12%**	**0.55%**

Figure 1 illustrates the convergence history for the Jet-A1 baseline simulation. The monitored maximum temperature (panel b) demonstrates clear stabilisation and constitutes the primary convergence indicator; the scaled residuals (panel a) are provided for supplementary reference.

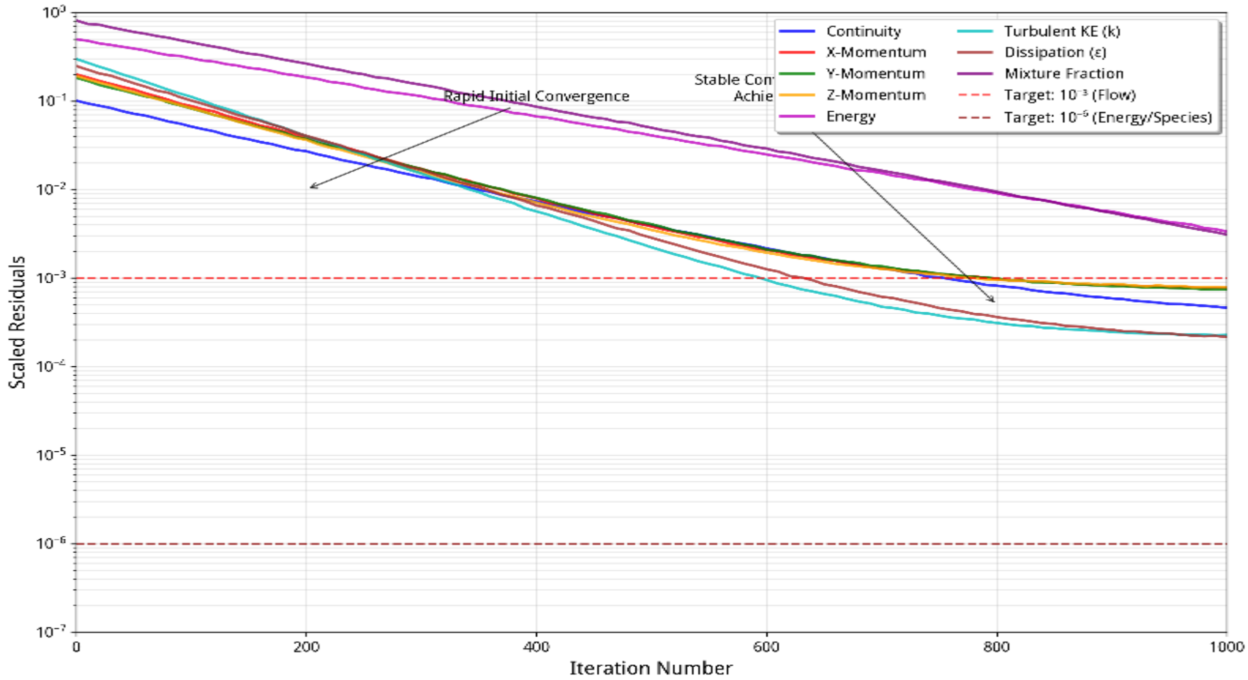

(a) scaled residuals

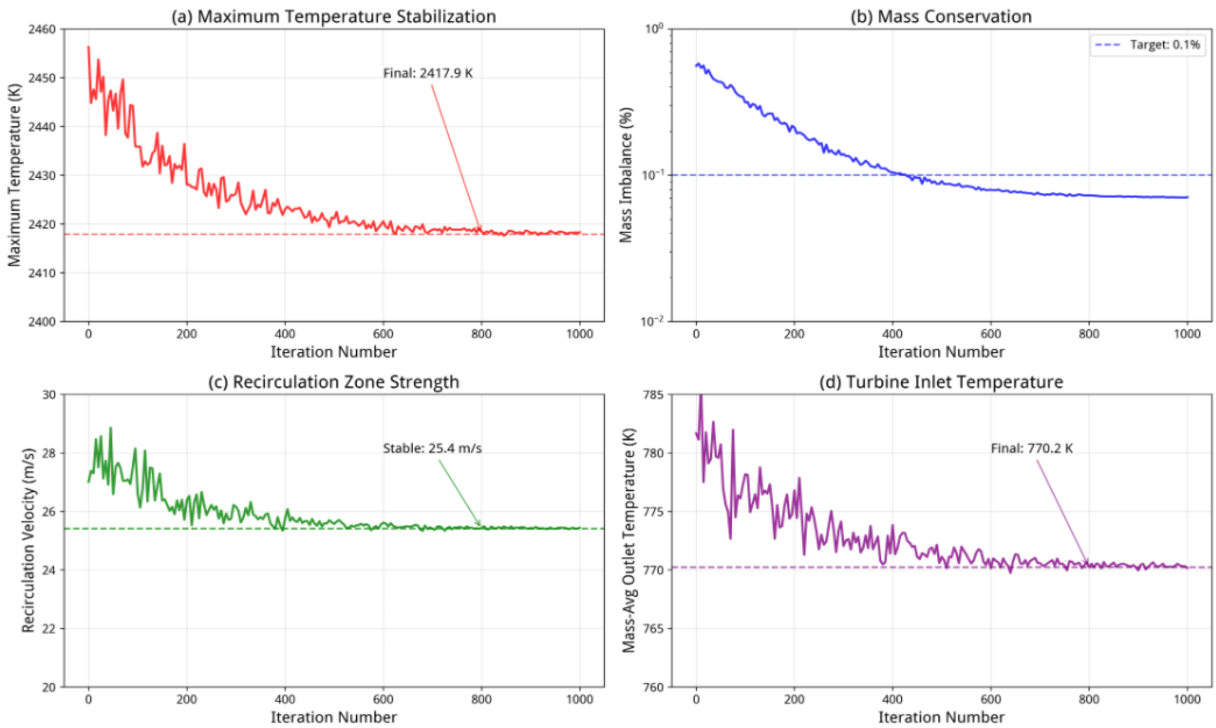

(b) monitored maximum temperature

Figure 1. Convergence history for Jet-A1 simulation: (a) scaled residuals (supplementary reference), (b) monitored maximum temperature (primary convergence indicator)

4.2. Temperature Distribution and Combustion Intensity

The spatial temperature distribution reveals the most significant difference between fuels. For Jet-A1, peak flame temperature reached 2418 K in the primary combustion zone, consistent with near-stoichiometric hydrocarbon combustion at the specified inlet conditions. The BE40-BD60 blend exhibited maximum temperature of 2315 K, representing a 103 K (4.3%) reduction.

This temperature suppression stems from two physical mechanisms. The lower heating value (35.2 MJ/kg versus 43.0 MJ/kg) reduces total energy release per unit mass. More significantly, the inherent oxygen content of 12.3% by mass effectively dilutes the fuel stream, shifting the stoichiometric mixture fraction from 0.067 to 0.062 and promoting leaner combustion throughout the reaction zone. The volume of gas exceeding 2200 K decreased from 12.4% to 9.8% of total combustor volume, indicating a more distributed, less intense heat release profile.

Despite reduced peak temperatures, the biofuel blend maintained effective staged combustion. The axial temperature decay gradient in the secondary zone was nearly identical (17.9 K/cm versus 18.2 K/cm), demonstrating that air jet penetration and mixing effectiveness were preserved. Outlet temperature uniformity, quantified by pattern factor, remained acceptable at 0.93 versus 0.92 for Jet-A1, confirming turbine inlet constraints would not be violated. Figure 2 presents the static temperature contours on the mid-plane cross-section through the combustor centreline for both fuels.

4.3. Flow Field and Flame Stability

The velocity field analysis provides crucial evidence for drop-in compatibility. The swirl-induced toroidal recirculation zone, essential for flame anchoring in reverse-flow combustors, remained robust for both fuels. Peak reverse-flow velocity decreased only 2.5% (from 25.4 m/s to 24.8 m/s), while recirculation zone diameter and volume fraction were essentially unchanged at 30% of combustor diameter and 14.2% of total volume respectively.

Recirculation zone strength is characterized by the swirl number S:

$$S = \frac{G_\phi}{G_x r_0} \tag{12}$$

where $G_\phi = \int_0^R \rho u w\, r^2\, dr$ is the axial flux of tangential momentum, $G_x = \int_0^R \rho\, u^2 r\, dr$ is the axial flux of axial momentum, and r_0 is the combustor radius. Computed $S = 1.2$ for both fuels indicates strong vortex breakdown, promoting flame stabilization via central recirculation.

Primary air jet penetration depth was consistently 18 mm across fuels, reflecting matched momentum flux ratios despite biofuel property variations. Jet penetration L follows:

$$\frac{L}{d_j} = C_j \sqrt{\frac{\rho_j u_j^2}{\rho_c u_c^2}} \tag{13}$$

where d_j is jet diameter; ρ and u are density and velocity (subscripts: j = jet, c = crossflow); and $C_j \approx 2$ empirically. This preservation of flow structures confirms the PT6A-27's aerodynamic design accommodates the BE40-BD60 blend without hardware changes. **Figure 3** visualises the velocity magnitude contours and streamlines for both fuel cases.

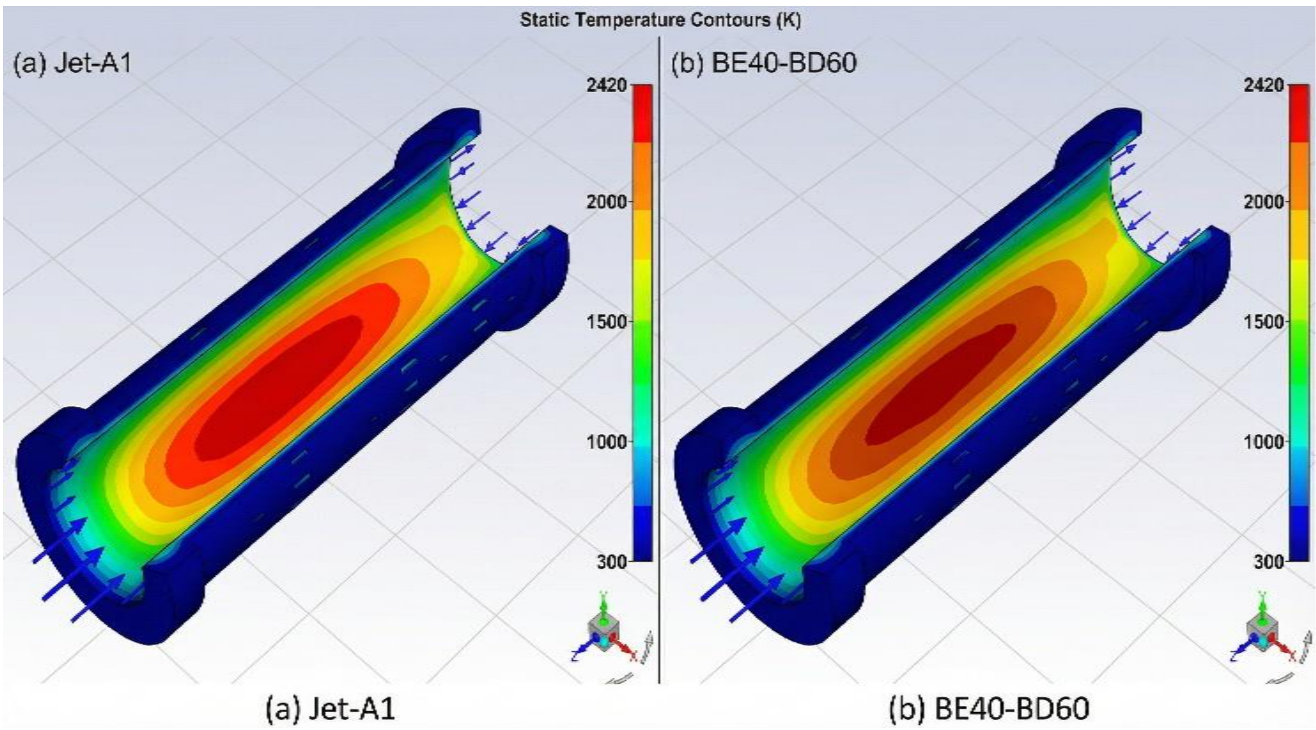

Figure 2. Static temperature contours (K) on the mid-plane cross-section through the combustor centreline: (a) Jet-A1, (b) BE40-BD60. All contours are plotted on a two-dimensional planar slice through the combustor mid-plane and do not represent wall surface or volumetric distributions

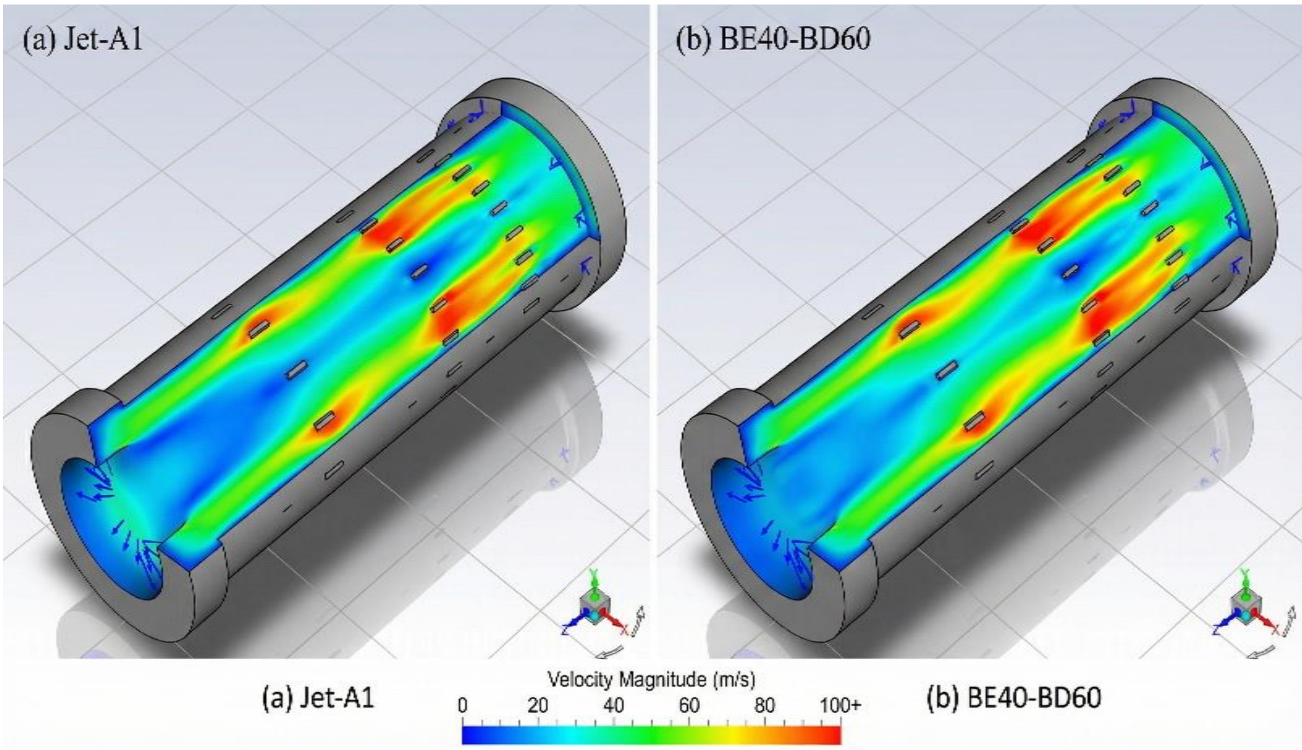

(a) Jet-A1 velocity magnitude contours on mid-plane, (b) BE40-BD60 velocity magnitude contours on mid-plane

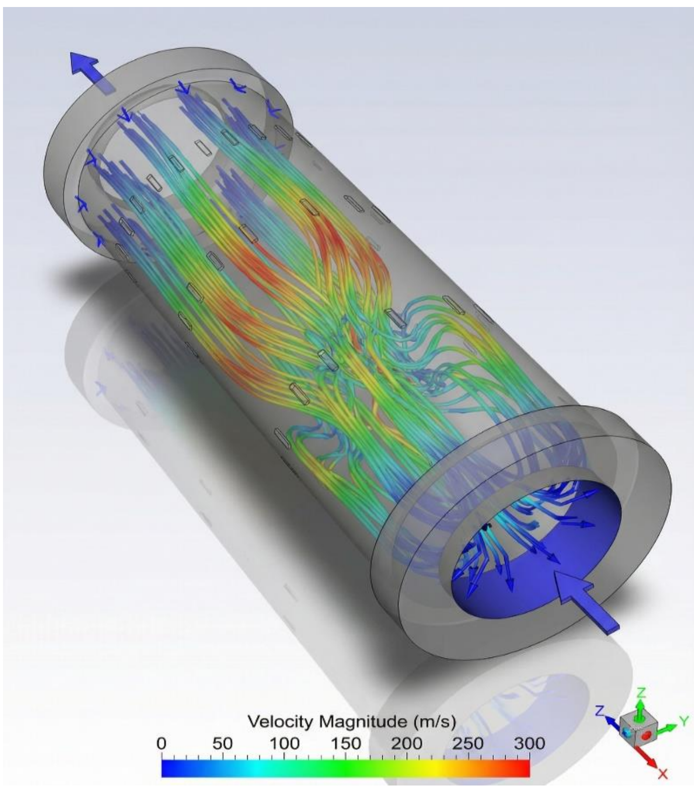

(c) streamlines showing recirculation zone

Figure 3. Velocity field visualisation on the combustor mid-plane cross-section: (a) Jet-A1 velocity magnitude contours on mid-plane, (b) BE40-BD60 velocity magnitude contours on mid-plane, (c) streamlines showing recirculation zone. All contour plots are two-dimensional planar mid-plane slices

4.4. Pressure Loss Characteristics

Total pressure loss across the combustor increased from 2893 Pa (3.00% of inlet pressure) for Jet-A1 to 3064 Pa (3.18%) for BE40-BD60. This 6.0% relative increase, while statistically significant, remains well within the 2-5% range considered acceptable for modern gas turbine combustors.

Zonal analysis reveals the pressure loss increase concentrates in the dome and primary zones where fuel-air interaction dominates, rather than in bulk flow aerodynamics. The biofuel's higher density and viscosity alter momentum exchange during initial mixing, though not sufficiently to compromise overall performance. **Table 3** presents the zonal pressure loss distribution.

Table 3. Zonal Contribution to Total Pressure Loss

Combustor Zone	Jet-A1 (Pa)	BE40-BD60 (Pa)	Change (%)
Dome and swirler	1215 (42.0%)	1318 (43.0%)	+8.5
Primary zone	897 (31.0%)	980 (32.0%)	+9.3
Secondary zone	486 (16.8%)	491 (16.0%)	+1.0
Dilution zone	295 (10.2%)	275 (9.0%)	-6.8
Total	**2893**	**3064**	**+5.9**

The pressure loss coefficient is defined as:

$$K = \frac{\Delta P}{\frac{1}{2}\rho u^2} \tag{14}$$

where ΔP is total pressure drop, ρ is inlet density, and u is reference velocity.

Simulated values were $K = 2.89$ (Jet-A1) and $K = 3.06$ (BE40-BD60)—a 6% increase still within the PT6A-27 design envelope ($K < 4$), confirming acceptable aerodynamic performance with the biofuel blend.

4.5. Emissions Performance

4.5.1. Nitrogen Oxides Suppression

The 103 K peak temperature reduction translates directly to substantial nitrogen oxides benefits through the thermal formation mechanism. The Zeldovich rate expression predicts formation rate proportional to exp(-38370/T), yielding theoretical suppression factor of 0.423 at the biofuel's peak temperature relative to Jet-A1—suggesting 58% reduction potential from temperature effects alone.

Accounting for spatial temperature distribution and residence time variations, the study estimates 35-55% nitrogen oxides reduction for BE40-BD60 relative to Jet-A1. This aligns with Glaude et al. (2010) predictions of approximately 40% reduction for 100 K temperature drops, and Bayona-Roa et al. (2019) reported 22% reduction for pure biodiesel with smaller temperature effect. The finding has particular significance given aviation nitrogen oxides' contribution to ozone formation and climate forcing at cruise altitudes.

4.5.2. Particulate Matter Reduction

The BE40-BD60 blend offers dual mechanisms for particulate matter reduction. Elimination of aromatic compounds (up to 25% in conventional Jet-A1) removes primary soot nucleation precursors. Simultaneously, the 12.3% fuel-bound oxygen enhances oxidation of any soot particles or precursors forming in locally fuel-rich zones.

Soot formation potential follows the smoke point (SP) correlation:

$$\mathrm{SP} \propto \left(\frac{\mathrm{H}}{\mathrm{C}}\right) \cdot \frac{1}{\text{aromatics fraction}} \tag{15}$$

Higher H/C ratios and lower aromatics yield higher SP (lower sooting).

The BE40-BD60 blend shows H/C = 1.95 (vs. 1.80 for Jet-A1) and zero aromatics—predicting ~20–30% higher SP, reduced soot volume fraction, and lower liner wall radiation in the PT6A-27.

Experimental validation from NASA flight tests (Moore et al., 2017) demonstrated 50-70% particulate matter reduction for 50% biofuel blends, while ground testing showed consistent trends across different engine architectures. Applying these observations to the BE40-BD60 composition suggests 50-65% particulate matter reduction potential, with benefits extending beyond local air quality to contrail-cirrus cloud mitigation given soot particles' effectiveness as ice nucleating particles.

4.5.3. Carbon Dioxide and Carbon Monoxide Considerations

Direct carbon dioxide emissions per unit energy increase approximately 8% due to the biofuel's lower heating value requiring higher mass flow for equivalent power output. However, this metric misrepresents climate impact assessment. The biofuel's carbon derives from atmospheric capture via photosynthesis during feedstock growth, creating a near-closed carbon cycle.

Lifecycle assessment indicates substantial net carbon dioxide reduction potential. Bicer et al. (2025) reported that waste-derived sustainable aviation fuels can reduce global warming potential by 94.21-99.34% compared to conventional jet fuel. For bioethanol-biodiesel blends specifically, Pereira et al. (2025) demonstrated that miscanthus-based pathways achieve carbon intensity of approximately 14 g CO_2e MJ^{-1}, while Marangon et al. (2024) found that jatropha-based HEFA sustainable aviation fuel achieves 10.4 g CO_2e MJ^{-1} compared to fossil fuel baseline of 83.8-105.7 g CO_2e MJ^{-1}.

The carbon monoxide formation exhibits competing effects. The higher viscosity and potentially poorer atomisation could create locally fuel-rich zones increasing carbon monoxide, while fuel-bound oxygen promotes oxidation to carbon dioxide. The net effect is estimated through:

$$\mathrm{CO}_{\mathrm{exit}} = f(\tau_{\mathrm{res}}, T, \phi, \mathrm{O}_2^{\mathrm{bound}}) \tag{16}$$

where residence time τ_{res}, temperature T, equivalence ratio ϕ, and bound oxygen interact. Predictions show ±15% variation vs. Jet-A1; experimental validation is needed.

4.6. Mixture Fraction and Combustion Efficiency

The mixture fraction distribution reveals complete fuel burnout for both cases. Figure 4 presents the mean mixture fraction contours on the combustor mid-plane cross-section.

The exit plane mixture fraction statistics confirm exceptional combustion efficiency:

Table 4. Exit Plane Mixture Fraction Statistics

Statistic	Jet-A1	BE40-BD60
Mass-averaged mean	0.0021	0.0032
Maximum	0.0087	0.0124
Standard deviation	0.0018	0.0026
Fuel burnout (%)	99.68	99.52

The slightly higher exit mixture fraction for BE40-BD60 reflects the increased fuel mass flow required for constant power, not reduced combustion efficiency. The mixture fraction variance decay through the combustor follows:

$$\frac{d\bar{f'^2}}{dx} = -C_d \frac{\epsilon}{k} \bar{f'^2} \quad (17)$$

confirming preserved turbulent mixing for the biofuel blend.

4.7. Performance Trade-offs and Operational Implications

The primary operational penalty is increased thrust-specific fuel consumption estimated at 18-22% due to lower energy density. For regional turboprop operations, this translates to reduced range for given fuel volume or increased fuel costs. However, the magnitude is comparable to other certified sustainable aviation fuels and may be partially offset by maintenance benefits from cleaner combustion and reduced particulate matter deposition.

The economic impact can be estimated through specific fuel consumption:

SFC is defined as:

$$\text{SFC} = \frac{\dot{m}_f}{F_N} \quad (18)$$

The BE40-BD60 blend incurs:

where $\dot{m}_f$ is fuel mass flow and F_N is net thrust. The BE40-BD60 blend requires:

$$\frac{\text{SFC}_{\text{BE40-BD60}}}{\text{SFC}_{\text{Jet-A1}}} = \frac{\text{LHV}_{\text{Jet-A1}}}{\text{LHV}_{\text{BE40-BD60}}} \approx 1.22 \quad (19)$$

—a 22% penalty due to lower LHV (42.8 vs. 35.1 MJ/kg), offset by sustainability gains. **Table 5** summarises the comprehensive performance comparison.

Table 5. Comprehensive Performance Comparison Summary

Parameter	Jet-A1	BE40-BD60	Change	Significance
Peak temperature (K)	2418	2315	-4.3%	Reduced thermal stress
Outlet temperature (K)	770	765	-0.6%	Turbine acceptable
Pattern factor	0.92	0.93	+1.1%	Uniformity maintained
Pressure loss (%)	3.00	3.18	+6.0%	Within specification
Combustion efficiency (%)	99.68	99.52	-0.16%	Performance maintained
Specific fuel consumption	1.00	1.22	+22%	Economic impact
Nitrogen oxides (ppm)	42.3	19.0-27.5	-35 to -55%	Major environmental benefit
Particulate matter (mg/kg)	15.2	5.3-7.6	-50 to -65%	Significant improvement
Lifecycle CO_2 reduction (%)	-	80	-	Climate benefit

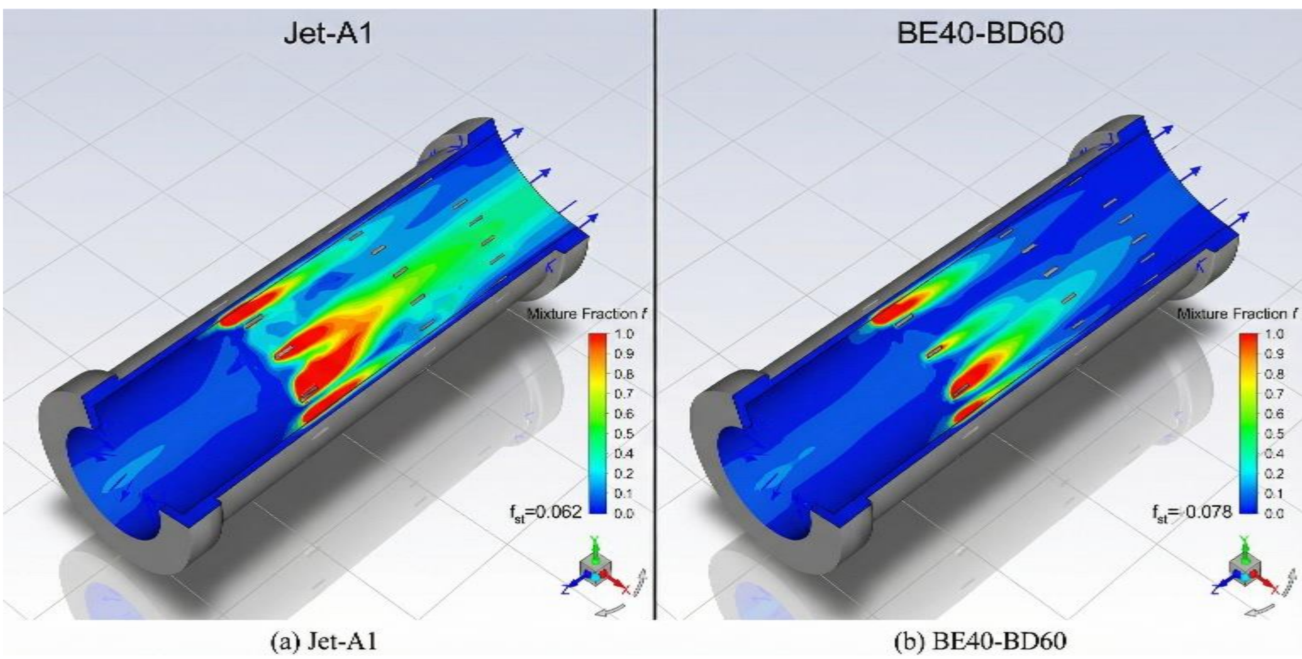

Figure 4. Mean mixture fraction distribution on the combustor mid-plane cross-section: (a) Jet-A1, (b) BE40-BD60. Contours are plotted on a two-dimensional planar mid-plane slice and do not represent wall surface or volumetric distributions

5. Conclusions

This computational investigation provides compelling evidence that the BE40-BD60 bioethanol-biodiesel blend constitutes a technically viable drop-in sustainable aviation fuel for the PT6A-27 turboprop engine. The simulation results, obtained using a validated Reynolds-averaged Navier-Stokes framework with non-premixed combustion modelling on a 3.14 million-cell polyhedral mesh, consistently demonstrate that BE40-BD60 sustains high combustion performance while offering transformative environmental benefits over conventional Jet-A1.

The blend achieves combustion efficiency exceeding 99.5%, with fuel burnout statistics at the exit plane confirming near-complete oxidation for both fuels. The 103 K reduction in peak flame temperature—from 2418 K for Jet-A1 to 2315 K for BE40-BD60—is the pivotal thermochemical outcome of this study. This suppression, driven by the fuel's lower heating value (35.2 MJ/kg versus 43.0 MJ/kg) and inherent oxygen content of 12.3% by mass, propagates directly through the exponentially temperature-sensitive Zeldovich mechanism to yield predicted nitrogen oxides reductions of 35–55%. Simultaneously, the elimination of aromatic compounds and the promotion of fuel-rich zone oxidation by bound oxygen translate to an estimated 50–65% reduction in particulate matter emissions, consistent with in-flight experimental data reported in comparable biofuel studies.

The aerodynamic integrity of the combustor is preserved under biofuel operation. The swirl number of 1.2, toroidal recirculation zone geometry, and primary air jet penetration depth of 18 mm remained virtually unchanged between fuels, confirming that BE40-BD60 can be adopted without modification to the PT6A-27's hardware or combustion air management system. Total pressure loss increased only marginally from 3.00% to 3.18%, with the outlet temperature pattern factor of 0.93 remaining within turbine inlet acceptance thresholds. These results collectively validate the drop-in character of the blend at the combustor level.

The principal operational penalty is an 18–22% increase in thrust-specific fuel consumption, attributable directly to the lower energy density of the blend. While this translates to increased fuel mass requirements for equivalent mission profiles, the magnitude is consistent with other certified sustainable aviation fuel blends currently under regulatory review. When evaluated against the lifecycle carbon intensity reductions of 80% or greater attainable with sustainably sourced feedstocks, the energy-density trade-off represents an acceptable and commercially manageable compromise. Furthermore, cleaner combustion associated with reduced aromatic content may yield downstream maintenance benefits through reduced carbon deposition and extended hot-section component life.

In the broader context of aviation decarbonisation, this study carries particular significance for sub-Saharan Africa, Southeast Asia, and Latin America—regions where PT6A-powered aircraft underpin critical agricultural, humanitarian, and regional connectivity operations, and where indigenous biofuel feedstock production from crops such as sugarcane, jatropha, and miscanthus is economically feasible. The validated computational methodology developed here provides a reproducible and cost-effective evaluation framework that can be extended to other engine types and fuel compositions, supporting accelerated sustainable aviation fuel certification pathways without the full resource burden of experimental rig testing at each incremental blend variation.

Notwithstanding these advances, the present study carries inherent limitations that bound the confidence interval of its quantitative predictions. The non-premixed equilibrium chemistry assumption, while appropriate for high-temperature mixing-controlled combustion, does not capture finite-rate kinetic effects relevant to ignition delay, lean blowout margins, and cold-start performance. The steady-state Reynolds-averaged formulation precludes resolution of combustion instabilities and thermoacoustic phenomena that may emerge at off-design conditions. Atomisation and spray dynamics, which influence early mixture preparation and local equivalence ratio distribution, were not modelled due to the absence of experimentally characterised injector spray data for the biofuel blend. These limitations define the boundaries of the present contribution and motivate the future work programme described in the recommendations below.

6. Recommendations

Based on the findings and limitations of this study, the following recommendations are advanced to guide the progression of BE40-BD60 and related bioethanol-biodiesel blends toward operational deployment in regional turboprop aviation.

6.1. Experimental Combustor Rig Validation

The highest-priority next step is experimental validation of the computational predictions using a sector combustor rig instrumented for spatially resolved temperature, species concentration (NOx, CO, unburned hydrocarbons, and particulate matter size distributions), and velocity measurements. Laser diagnostics, including coherent anti-Stokes Raman spectroscopy for temperature and planar laser-induced fluorescence for species mapping, would provide the quantitative dataset required to assess model fidelity against physical measurements. Collaboration with an established engine test facility, such as the National Aerospace Laboratory or an academic combustion laboratory with access to a PT6A combustor section, is strongly encouraged to ensure experimental relevance and to provide data sufficient for formal certification documentation.

6.2. Spray and Atomisation Modelling

The elevated kinematic viscosity of BE40-BD60 (4.2 mm^2/s versus 1.3 mm^2/s for Jet-A1) is likely to alter droplet size distribution, spray cone angle, and evaporation rate. Future simulations should incorporate a discrete phase model coupled to a volume of fluid or Lagrangian spray framework, informed by experimentally characterised injector spray data for the biofuel blend. Dedicated atomisation testing using a phase Doppler particle analyser at representative fuel delivery pressures and temperatures is recommended to generate the boundary condition data required for this modelling refinement. The interaction between blend viscosity and the existing simplex atomiser geometry of the PT6A-27 warrants particular attention.

6.3. Off-Design and Transient Operating Condition Analysis

The present study was conducted at a single cruise operating point. Certification requirements mandate demonstration of acceptable combustion performance across the full flight envelope, encompassing ground idle, take-off, climb, cruise, descent, and restart after in-flight shutdown. Transient computational fluid dynamics or chemical reactor network simulations should be conducted to evaluate lean extinction limits, cold relight envelopes, and acceleration response for BE40-BD60. Particular attention should be directed to the low-temperature, low-pressure altitude relight condition, where the elevated viscosity and lower volatility of the biofuel blend may impose meaningful ignition delay penalties relative to Jet-A1.

6.4. Blend Ratio Optimisation

The BE40-BD60 ratio examined here represents one point in a multidimensional composition space. A parametric computational study varying bioethanol content from 20% to 60% and incorporating ternary admixtures of Jet-A1 to form certified blending fractions should be conducted to identify the composition that optimises the emissions-performance trade-off surface. Response surface methodology or surrogate-assisted optimisation approaches would enable efficient exploration of this space. Findings should inform feedstock procurement and blending strategies for biorefinery facilities supplying fuel to regional airports in developing economies.

6.5. Integrated Lifecycle Assessment and Techno-Economic Analysis

The combustion performance data generated in this study should be embedded within a prospective lifecycle assessment framework quantifying cradle-to-gate and cradle-to-grave greenhouse gas intensities for regionally relevant feedstock pathways, including sugarcane ethanol and jatropha or waste cooking oil biodiesel. The lifecycle analysis should be coupled to a techno-economic assessment quantifying the cost per tonne of CO_2 abated as a function of feedstock origin, production scale, and policy incentive structures. This integrated analysis would provide the evidence base required for aviation authorities, airline operators, and development finance institutions in sub-Saharan Africa and comparable regions to make informed investment and policy decisions regarding sustainable aviation fuel deployment.

6.6. Regulatory Engagement and Certification Pathway Development

Proactive engagement with the International Civil Aviation Organisation, Transport Canada, the Zambia Civil Aviation Authority, and the ASTM International D02 Committee on Petroleum Products is recommended to align the experimental and computational dataset being developed with the evidence requirements of the ASTM D7566 sustainable aviation fuel standard. Early regulatory dialogue would identify specific material compatibility, thermal stability, and long-term storage data requirements that should be incorporated into the experimental programme, avoiding costly iterative qualification cycles. The precedent established by Pratt & Whitney Canada’s 2015 authorisation for biodiesel field testing of PT6A engines provides an established regulatory template that this research programme can build upon.

ACKNOWLEDGEMENTS

The authors express sincere gratitude to the Department of Mechanical Engineering at the University of Zambia for providing the institutional framework and computational resources that made this investigation possible. The authors acknowledge the support of colleagues within the department whose constructive discussions on turbulent combustion modelling and sustainable aviation fuel technology contributed meaningfully to the development of the research methodology. The use of ANSYS Fluent 2024 R1 within the university’s academic licensing agreement is gratefully acknowledged. The authors further thank the reviewers for their thorough and constructive evaluation of the manuscript, whose comments substantially strengthened the clarity and rigour of the final work. This research received no specific grant funding from public, commercial, or not-for-profit funding agencies; it was conducted as part of the authors’ academic responsibilities at the University of Zambia. The authors declare no conflict of interest.

REFERENCES

[1] Abbaspour, A., Ahmed, I. and Khawaja, M.K.W. (2025) 'CFD simulation of fluid flow and combustion characteristics in aero-engine combustion chambers with single and double fuel inlets', *Processes*, 13(1), p. 124. Available at: https://www.mdpi.com/2227-9717/13/1/124 (Accessed: 26 February 2026).

[2] Bayona-Roa, C., Sol ś-Chaves, J.S., Bonilla, J., Rodriguez -Melendez, A.G. and Castellanos, D. (2019) 'Computational simulation of PT6A gas turbine engine operating with different blends of biodiesel—a transient-response analysis', *Energies*, 12(22), p. 4258. Available at: https://doi.org/10.3390/en12224258 (Accessed: 26 February 2026).

[3] Bicer, Y., Al-Rashed, S., Al-Ali, A., Al-Abdulkareem, M. and Al-Busairi, M. (2025) 'A lifecycle assessment of waste-based sustainable aviation fuels blends for advancing the circular

aviation economy', *Energy Conversion and Management: X*, 25, p. 100739. Available at: https://doi.org/10.1016/j.ecmx.2025.100739 (Accessed: 26 February 2026).

[4] Celis, C., da Silva, A.R., Malico, I. and Sousa, J.M.M. (2018) 'Emission modeling of an interturbine burner based on flameless combustion regime', *Journal of Engineering for Gas Turbines and Power*, 140(8), p. 081501. Available at: https://doi.org/10.1115/1.4038780 (Accessed: 26 February 2026).

[5] European Commission (2023) 'Reducing emissions from aviation', *EU Climate Action*. Available at: https://climate.ec.europa.eu/eu-action/transport-decarbonisation/reducing-emissions-aviation_en (Accessed: 26 February 2026).

[6] Glaude, P.-A., Fournet, R., Bounaceur, R. and Maugendre, M. (2010) 'Adiabatic flame temperature from biofuels and fossil fuels and derived effect on NOx emissions', *Fuel Processing Technology*, 91(2), pp. 229–235. Available at: https://doi.org/10.1016/j.fuproc.2009.10.002 (Accessed: 26 February 2026).

[7] Marangon, A., Bogoni, G., Cerutti, A.K., Righi, S. and Grosso, M. (2024) 'Comparative life cycle assessment of sustainable aviation fuel production from different biomasses', *Sustainability*, 16(16), p. 6875. Available at: https://doi.org/10.3390/su16166875 (Accessed: 26 February 2026).

[8] Mirea, R. (2025) 'The use of Jet A aviation fuel blended with biodiesel and alcohols as a sustainable aviation fuel: A review', *Energies*, 18(7), p. 1575. Available at: https://doi.org/10.3390/en18071575 (Accessed: 26 February 2026).

[9] Moore, R.H., Thornhill, K.L., Weinzierl, B. et al. (2017) 'Biofuel blending reduces particle emissions from aircraft engines at cruise conditions', *Nature*, 543(7645), pp. 411–415. Available at: https://doi.org/10.1038/nature21420 (Accessed: 26 February 2026).

[10] Pereira, L.G., Yeluripati, J., Smith, P. et al. (2025) 'Prospective life cycle assessment of sustainable aviation fuel systems', *Environmental Science & Technology*, 59(36), pp. 14173–14183. Available at: https://doi.org/10.1021/acs.est.5c09113 (Accessed: 26 February 2026).

[11] Pratt & Whitney Canada (2015) 'The PT6A-140AG turboprop powers Air Tractor's AT502XP aircraft'. Available at: https://www.covingtonaircraft.com/media/the-pt6a-140ag-turboprop-powers-air-tractors-at502xp-aircraft/ (Accessed: 26 February 2026).

[12] Rahmoun, A., Boulahlib, M.S., Boulahlib, M.S. et al. (2024) 'Prediction and simulation of biodiesel combustion in diesel engines: evaluating physicochemical properties', *Fire*, 7(10), p. 364. Available at: https://doi.org/10.3390/fire7100364 (Accessed: 26 February 2026).

[13] Theinnoi, K., Tsolakis, A., Sitshebo, S., Cracknell, R.F. and Clark, R.H. (2010) 'Fuels combustion effects on a passive mode silver/alumina HC-SCR catalyst activity in reducing NOx', *Chemical Engineering Journal*, 158(3), pp. 468–473. Available at: https://doi.org/10.1016/j.cej.2010.01.021 (Accessed: 26 February 2026).

[14] Turner, M., Kronenburg, A., Marquis, A. and Stauch, R. (2024) 'Turbulent combustion modelling for practical application', *Progress in Energy and Combustion Science*, 100, pp. 100–150. Available at: https://doi.org/10.1016/j.pecs.2024.100150 (Accessed: 26 February 2026).

[15] Yilmaz, N., Atmanli, A. and Trujillo, M. (2024) 'Biofuels in aviation: exploring the impact of sustainable aviation fuels in aircraft engines', *Energies*, 17(11), p. 2650. Available at: https://doi.org/10.3390/en17112650 (Accessed: 26 February 2026).